# Estimation of Spinal Loading During Manual Materials Handling Using Inertial Motion Capture

Larsen, Frederik Greve; Svenningsen, Frederik Petri; Andersen, Michael Skipper; de Zee, Mark; Skals, Sebastian Laigaard

*Published in:*
Annals of Biomedical Engineering

*DOI (link to publication from Publisher):*
10.1007/s10439-019-02409-8

*Publication date:*
2020

*Document Version*
Accepted author manuscript, peer reviewed version

## 1. Title Page

**Title:** Estimation of spinal loading during manual materials handling using inertial motion capture

**Abbreviated title:** Estimation of spinal loading using inertial motion capture

**Authors:** Frederik G. Larsen[a], Frederik P. Svenningsen[a], Michael Skipper Andersen[b], Mark de Zee[a] and Sebastian Skals[a,c*]

**Departments:** [a]Sport Sciences, Department of Health Science and Technology, Aalborg University, Aalborg, Denmark; [b]Department of Materials and Production, Aalborg University, Denmark; [c]Musculoskeletal Disorders, National Research Centre for the Working Environment, Copenhagen, Denmark

***Corresponding author:**

Sebastian Skals

National Research Centre for the Working Environment

Lersø Parkallé 105, 2100 Copenhagen East, Denmark

Phone: +45 39 16 52 85

E-mail: sls@nfa.dk

This is a pre-print of an article published in Annals of Biomedical Engineering. The final authenticated version is available online at: https://doi.org/10.1007/s10439-019-02409-8.

**Nomenclature**

| | |
|---|---|
| GRF&Ms | Ground reaction forces and moments |
| IMC | Inertial motion capture |
| JRF | Joint reaction force |
| IDA | Inverse dynamic analysis |
| OMC | Optical motion capture |
| GRF | Ground reaction force |
| IMU | Inertial measurement unit |
| OMC-MGRF | Optical motion capture with measured ground reaction forces |
| OMC-PGRF | Optical motion capture with predicted ground reaction forces |
| IMC-PGRF | Inertial motion capture with predicted ground reaction forces |
| GRM | Ground reaction moment |
| %BW | Percentage of body weight |
| %BW*BH | Percentage of body weight times body height |
| RMSE | Root-mean-square error |
| rRMSE | Relative root-mean-square error |
| ICC | Intraclass correlation coefficient |
| LoA | Limits of agreement |

## 2. Abstract and key terms

Musculoskeletal models have traditionally relied on measurements of segment kinematics and ground reaction forces and moments (GRF&Ms) from marked-based motion capture and floor-mounted force plates, which are typically limited to laboratory settings. Recent advances in inertial motion capture (IMC) as well as methods for predicting GRF&Ms have enabled the acquisition of these input data in the field. Therefore, this study evaluated the concurrent validity of a novel methodology for estimating the dynamic loading of the lumbar spine during manual materials handling based on a musculoskeletal model driven exclusively using IMC data and predicted GRF&Ms. Trunk kinematics, GRF&Ms, L4-L5 joint reaction forces (JRFs) and erector spinae muscle forces from 13 subjects performing various lifting and transferring tasks were compared to a model driven by simultaneously recorded skin-marker trajectories and force plate data. Moderate to excellent correlations and relatively low magnitude differences were found for the L4-L5 axial compression, erector spinae muscle and vertical ground reaction forces during symmetrical and asymmetrical lifting, but discrepancies were also identified between the models, particularly for the trunk kinematics and L4-L5 shear forces. Based on these results, the presented methodology can be applied for estimating the relative L4-L5 axial compression forces under dynamic conditions during manual materials handling in the field.

**Key terms:** Musculoskeletal modelling; inertial motion capture; inverse dynamic analysis; predicted ground reaction forces and moments; manual materials handling; low back loading.

## 3. Introduction

Manual material handling tasks, such as lifting, imposes high compression and shear forces on the spine[42], which can cause damage to ligaments, facet joints, muscles, nerve roots, and vertebral endplates[7,8]. However, the assessment of spinal loads *in vivo* is challenging and rarely performed due to the invasive methods involved[42]. For this reason, several other methods have been developed to estimate these forces, including two- and three-dimensional musculoskeletal models[9].

For example, De Zee et al.[44] designed a generic, detailed musculoskeletal model of the spine with seven rigid segments that can be incorporated in inverse dynamic analysis (IDA) to estimate the internal loading of the spinal column. The validity of the generic spine model has been extensively investigated, showing good agreement with *in vivo* intradiscal pressure measurements between the L4-L5 discs during lifting[4,30,31,44].

The quantification of body kinematics and kinetics for IDA of manual materials handling would ideally be performed in the field, since laboratory experiments typically involve simplifying and constraining movements to some extent. Traditionally, IDA would involve optical motion capture (OMC) and floor-mounted force plates[11] or instrumented force shoes[40]. However, due to recent developments of methods to predict ground reaction forces and moments (GRF&Ms), the application of IDA in the field mainly depends on one's capability to obtain accurate segment kinematics[13,21,22,36,37].

Recent advances in ambulatory motion tracking systems, such as inertial motion capture (IMC), enables full-body motion capture in any working environment without the drawback from magnetic distortions[12,34]. Recent studies have evaluated the accuracy of IMC with promising results: for example, Koning et al.[23] found lower extremity peak joint angle errors up to 11 degrees for an IMC system compared to OMC during gait, squat and slide boarding, while Karatsidis et al.[22] found relative root-mean-square errors up to 36.9% and 38.0% for lower-body kinematics and kinetics during gait, respectively. However, the combination of ambulatory IMC measurements and musculoskeletal modelling for estimating spinal loads during manual materials handling needs to be specifically evaluated before it can be used in the field.

Therefore, the aim of the present study was to evaluate the concurrent validity of a musculoskeletal model driven exclusively using IMC data and GRF prediction for estimating L4-L5 spinal forces during various lifting and transferring tasks. To achieve this, we compared the joint reaction forces (JRFs) at the L4-L5 discs and the predicted GRF&Ms to an OMC and force plate-driven musculoskeletal model. The OMC and force plate driven model was considered a silver standard, as this is the most commonly used system for providing kinematic and kinetic input to musculoskeletal models. This approach will help determine if musculoskeletal models driven by IMC data and ground reaction force (GRF) prediction can be used to estimate spinal loading during manual materials handling tasks in the field with results comparable to the traditional laboratory-based approach.

## 4. Materials and Methods

### 4.1 Subjects

Thirteen healthy subjects (9 male and 4 female, age 25.7 ± 3.4 years, height 179.3 ± 7.8 m, weight 76.4 ± 12.8 kg) volunteered to participate in the study. The study followed the ethical guidelines of The North Denmark Regional Committee on Health Research Ethics and all subjects provided written informed consent prior to data collection.

### 4.2 Instrumentation

Motion analysis was performed using the OMC and IMC systems simultaneously. For the OMC system, the trajectories of 42 passive reflective markers were recorded with eight infrared Oqus cameras (Qualisys, Göteborg, Sweden), sampling at 120 Hz, using a full-body protocol. The marker protocol was similar to Karatsidis et al.[21] and is provided as supplementary material. For the IMC system, full-body kinematics were measured using the Xsens MVN Awinda wireless motion-tracker (Xsens Technologies BV, Enschede, The Netherlands), consisting of 17 inertial measurement units (IMUs) sampling at 60 Hz. The placement of the 17 strap-based IMUs is also provided as supplementary material. GRF&Ms were measured using three floor-mounted force plates (AMTI, Watertown, MA, USA), one placed beneath each foot sampling at 1200 Hz. All measurements were synchronized using a TTL trigger in Xsens MVN Analyze (v.2018.0.0).

### 4.3 Experimental procedures

The experimental procedures lasted approximately two hours. Initially, the IMUs and reflective markers were attached to the subjects. The IMC system includes a tight-fitting customized t-shirt and velcro straps for attaching the IMUs to the body. However, as a preventive measure for reducing soft-tissue artefacts associated with the reflective markers on the torso, the male subjects were asked to be shirtless during the measurements, while the female subjects were asked to wear a brassiere. However, the female subjects were not comfortable with only wearing a brassiere and were permitted to wear the t-shirt. For the male subjects, the shoulder, pelvis, and sternum IMUs were instead attached to the skin with double-sided tape and the other sensors were attached with the accompanying velcro straps. After placing the IMUs, the subjects' body dimensions (including body height, foot length, arm span, ankle height, hip height and width, knee height, shoulder width and height) were manually measured with a caliper and entered into the MVN software. Subsequently, the subjects were asked to stand in an upright standing neutral position (N-pose) and perform a short walking trial to calibrate the IMC system[34].

All subjects performed six different lifting tasks and two transferring tasks at their own pace, including symmetrical lifting, asymmetrical lifting, and load transferring, as illustrated in Fig. 1. The symmetrical lifting tasks involved lifting a box of different weights (5, 10, 15, and 20 kg) from the ground to an upright position and back to the starting point. Two-handed load transferring involved moving a box of 10 kg between two tables of 1 m in height. The tables were placed 0.2 m laterally to the right and left foot of the subject. Similarly, a one-hand transferring task was performed, where the subjects lifted a 5 kg weight with the right hand. The asymmetrical lifting tasks involved lifting a box with different weights (5 and 10 kg) from the floor to a table of 0.8 m in height. During these lifts, the table was placed 0.2 m laterally from the right foot of the subject. Three repetitions were performed for each task in a randomized order, totalling 24 lifts for each subject.

### 4.4 Model setup

From the laboratory measurements, three musculoskeletal models were developed: (1) OMC and measured GRF&Ms (OMC-MGRF), (2) OMC and predicted GRF&Ms (OMC-PGRF), and (3) IMC and predicted GRF&Ms (IMC-PGRF), as illustrated in Fig. 2.

The musculoskeletal models were developed in the AnyBody Modeling System v. 7.1 (AnyBody Technology A/S, Aalborg, Denmark) using the *Plug-in-gait-MultiTrial_StandingRef* as the template for the OMC-MGRF and OMC-PGRF models, while the *BVH_Xsens* was used as the template for the IMC-PGRF model. Both these template models are based on the common *AnyMocap* framework and are identical, except for the handling of the different input data. All templates were extracted from the Anybody Managed Model Repository v. 2.1.

The musculoskeletal models had a total of 44 degrees of freedom, including 2 x 3 DOF at the ankle joints, 2 x 1 at the knee joints, 2 x 3 at the hip joints, 6 DOF at the pelvis, 3 DOF between pelvis and thorax, 2 x 2 at the elbow joints, 2 x 3 at the glenohumeral joints, 2 x 3 at the sternoclavicular joints, 2 x 2 DOF at the wrist joints and 1 DOF at the neck joint. The lower extremity model was based on the cadaver study of Carbone et al.[6], the lumbar spine model was based on the work of de Zee et al.[44], Hansen et al.[18], and Han et al.[17], and the shoulder and arm models were based on the research of Van Der Helm et al.[19] and Veeger et al.[38,39]. The spine model was actuated by 188 muscle elements, modeled with non-linear disc stiffness in the lumbar region, and with ligaments and an intra-abdominal pressure applied similar to Han et al.[17]. All segments were modeled as rigid-bodies, and the spine model consisted of seven rigid segments describing the cervical, thorax, and lumbar vertebras as well as the sacrum[18,44]. The model followed a spine rhythm that distributes the trunk motion over the vertebral bodies using a coupled-mechanism[18].

**4.5 Model scaling**

For each subject, a single trial from the OMC data was used to scale the OMC-MGRF and OMC-PGRF models using the method of Andersen et al.[1,2]. The segment dimensions obtained from the single trial were subsequently saved and used to scale all other OMC trials. The IMC-PGRF model was scaled according to the manually measured segment dimensions through multiple steps. First, the stick figures were exported from the Xsens software as .bvh-files. Before processing the .bvh-files in the AnyBody Modeling System, the kinematics were pre-processed using forward kinematics to prevent singular rotations potentially arising due to the Cardan angle sequences employed in Xsens (see Skals et al.[37] for further details). Subsequently, the stick figures were imported into the AnyBody Modeling System together with the *BVH_Xsens* musculoskeletal

model. The *BVH_Xsens* model segment lengths were scaled according to the joint-to-joint distances of the stick figure contained in the .bvh-files. Since multiple body dimensions were not directly scalable from the stick figure, additional nodes were added to the unscaled segments of the musculoskeletal model (pelvis, foot, and trunk) at points that were identifiable on the stick figure. Then, the distance between the added nodes were computed and saved with the unscaled segment lengths, where after the ratio between the unscaled segments and the distance between the added nodes were multiplied onto the segment lengths on the stick figure before being applied to scale the *BVH_Xsens* musculoskeletal model.

To enable scaling and marker tracking between the two models, virtual markers were introduced on both the stick figure and the musculoskeletal model. A non-linear least-square optimization problem, which minimizes the least-square difference of the virtual markers between the two models, was applied to ensure optimal tracking[2]. Further details can be found in Skals et al.[37] and Karatsidis et al.[22]. Lastly, the body mass was linearly distributed to the segments according to the regression equations of Winter[43]. The reflective and inertial marker trajectories as well as the force measurements were digitally filtered using a fourth-order zero-phase Butterworth filter with a cut-off frequency set to 6 Hz for the marker trajectories and 15 Hz for the force plate measurements. A flowchart of the development of the three musculoskeletal models is illustrated in Fig. 2.

**4.6 Muscle recruitment**

Muscle recruitment was solved by formulating a third-order polynomial optimization problem that distributes the muscle forces:

$$\min G(\boldsymbol{f}^M) = \sum_{i=1}^{n^{(M)}} \left(\frac{f_i^{(M)}}{N_i^{(M)}}\right)^3 + \sum_{i=1}^{5n^{(C)}} \left(\frac{f_i^{(C)}}{N_i^{(C)}}\right)^3 + \sum_{i=1}^{n^{(R)}} \left(\frac{f_i^{(R)}}{N_i^{(R)}}\right)^3, \quad (1)$$

$$\boldsymbol{C}f = \boldsymbol{d},$$

$$0 \leq f_i^{(M)}, i = 1, \dots, n^{(M)},$$

$$0 \leq f_i^{(C)}, i = 1, \dots, 5n^{(C)},$$

$$0 \leq f_i^{(R)}, i = 1, \dots, n^{(R)}.$$

$G$ is the third-order polynomial objective cost function, $f_i^{(\mathrm{M})}$ is the *i*th muscle, $n^{(\mathrm{M})}$ the number of muscles, and $N_i^{(M)}$ is the strength of the muscle, $f_i^{(\mathrm{C})}$ is the *i*th contact force, $n^{(C)}$ is the number of contact elements, $N_i^{(C)}$ is the strength of the contact element, $f_i^{(R)}$ is the *i*th residual force, $n^{(R)}$ is the number of residual forces, $N_i^{(R)}$ is the strength of the residual force, $\mathbf{C}$ is the coefficient matrix for the dynamic equilibrium equations, $\mathbf{f}$ is all the unknown muscle and joint reaction forces, and $\mathbf{d}$ contains all the external and inertial forces. Furthermore, the non-negativity constraints dictate that the muscles can only pull. The muscles were modeled without contraction dynamics, and their strength determined from the physiological cross-sectional area and a mass-fat scaling law[14,32].

**4.7 Prediction of GRF&Ms**

GRF&Ms were predicted for the IMC-PGRF and OMC-PGRF models using a method that has been validated extensively in previous studies[13,22,36,37]. In short, 25 dynamic contact elements were attached under each foot of the musculoskeletal model, each consisting of five uniaxial force actuators that were able to generate a positive normal force, as well as positive and negative anteroposterior and mediolateral static friction forces. Furthermore, a non-linear strength function similar to that of Skals et al.[36] was implemented to ensure that the contact elements would only generate forces when they were close to the ground and almost stationary. Lastly, to improve numerical stability, small residual forces and moments were attached to the pelvis with a strength of 10 N and 10 Nm. The individual actuation of each contact force actuator was computed as part of the muscle recruitment problem.

**4.8 Data analysis**

The following variables were extracted from all musculoskeletal models: 1) trunk flexion, rotation and lateral flexion angle, 2) vertical GRF for the right and left foot, 3) JRFs at the L4-L5 discs, including axial compression, mediolateral and anteroposterior shear forces, and 4) erector spinae muscle force. Furthermore, anteroposterior and mediolateral GRFs, as well as transverse, sagittal, and frontal plane ground reaction moments (GRMs), which were recalculated in the ankle joint coordinate system for both right and left foot, are presented in the supplementary material. The GRFs and JRFs were normalized to percentage of body weight (%BW), while GRMs were normalized to percentage of body weight times body height (%BW*BH)[28]. The start and end

point of the lifting cycles were determined as the first instance where the lifted burden had no contact with the base of the starting position and the instance when the burden made contact with the base of the end position, respectively (see Fig. 1). For the symmetrical lifting task, the end position was the instance when the subjects were standing fully upright, i.e. the point of maximal torso extension. The kinematic and kinetic data for each lifting and transferring task were then resampled to 101 data points (one lifting cycle), where after each subject's three trials of each task were averaged.

To evaluate the agreement between the OMC-MGRF, OMC-PGRF, and IMC-PGRF models, several statistical analyses were performed. The absolute and relative agreement for all times-series curves were performed using root-mean-square error (RMSE) and relative root-mean-square error (rRMSE), similar to Ren et al.[33]. Furthermore, intraclass correlation coefficients (ICC) were calculated over all time-series points and categorized as $ICC \leq 0.5$ (poor), $0.50 \leq ICC \leq 0.75$ (moderate), $0.75 \leq ICC \leq 0.9$ (good), and $0.9 < ICC$ (excellent)[24,35]. Lastly, Bland-Altman bias and limits of agreement (LOA) were computed for the L4-L5 axial compression time-series signals, following the approach of Meldrum et al. [27], to test the agreement between the OMC-MGRF and the OMC-PGRF and IMC-PGRF models, as proposed by McLaughlin et al.[26] A Shapiro-Wilk test (statistical significance set to $p < 0.05$) showed that the L4-L5 axial compression time-series signals were not normally distributed, and therefore, a non-parametric Bland-Altman model was applied[5]. Instead of computing bias and LoA, which relies on normality, the median, $5^{th}$ and $95^{th}$ percentiles were computed.

## 5. Results

Time-series curves of the selected variables during all lifting conditions are depicted in Fig. 3, 4 and 5. The statistical comparisons of the IMC-PGRF and OMC-MGRF models as well as the OMC-PGRF and OMC-MGRF models are described in the following. However, the comparisons of the IMC-PGRF and OMC-PGRF models have been omitted from the text and tables for clarity, as these differences were almost identical to those found between the IMC-PGRF and OMC-MGRF models.

### 5.1 Trunk kinematics

Trunk flexion showed poor correlations between the IMC and OMC models (see Table 1) for both lifting and transferring tasks (ICC ranging from 0.20 to 0.41). Specifically, trunk lateral flexion showed poor correlations for all lifting conditions (ICC ranging from -0.08 to 0.41), while trunk rotations showed poor correlations for the symmetrical lifting tasks and asymmetrical lifting with 10 kg (ICC ranging from 0.01 to 0.47), but moderate to good correlations for asymmetrical lifting with 5 kg as well as for both transferring tasks (ICC ranging from 0.51 to 0.83). RMSE ranged from 6.86 to 16.54 degrees for trunk flexion, from 1.80 to 2.89 degrees for trunk lateral flexion, and 4.58 to 7.75 degrees for trunk rotation. During symmetrical lifting, rRMSE between the IMC and OMC models for all trunk kinematics ranged from 138.4% to 229.3%, while the values for the asymmetrical lifting and transferring tasks ranged from 16.03% to 246.5%.

### 5.2 Vertical GRFs

Vertical GRFs for the left and right foot showed moderate to good correlations (see Table 1) between the IMC-PGRF and OMC-MGRF models for the symmetrical lifting tasks (ICC ranging from 0.51 to 0.77), but excellent correlations during asymmetrical lifting and both transferring tasks (ICC ranging from 0.92 to 0.96). When comparing the OMC-PGRF and OMC-MGRF models (see Table 2), excellent correlations were found for all tasks (ICC ranging from 0.96 to 0.98), except for symmetrical lifting with 20 kg (ICC = 0.86). In addition, RMSEs ranged from 5.06%BW to 12.14%BW for IMC-PGRF compared to OMC-MGRF, while for OMC-PGRF compared to OMC-MGRF, the RMSEs ranged from 2.30%BW to 8.73%BW. The rRMSEs for IMC-PGRF versus OMC-MGRF and OMC-PGRF versus OMC-MGRF ranged from 10.29% to 34.14% and from 4.72% to 15.60%, respectively.

### 5.3 L4-L5 Joint reaction forces

The axial compression and anteroposterior shear forces showed moderate to excellent correlations during symmetrical and asymmetrical lifting (ICC ranging from 0.65 to 0.92), while the mediolateral shear force showed poor to moderate correlations (ICC ranging from 0.01 to 0.51) when comparing IMC-PGRF to OMC-MGRF (see Table 1). During one- and two-handed transferring, poor (ICC = 0.16) and moderate (ICC = 0.57) correlations were found for the axial compression force (ICC = 0.57), respectively. For both transferring tasks, moderate to good

correlations (ICC ranging from 0.74 to 0.78) were found for the anteroposterior shear force, while the mediolateral shear force showed poor correlations (ICC ranging from 0.04 to 0.23). When comparing the OMC-PGRF and OMC-MGRF models (see Table 2), excellent correlations were found for all L4-L5 JRFs during symmetrical and asymmetrical lifting (ICC ranging from 0.91 to 1), while good to excellent correlations were found for the transferring tasks (ICC ranging from 0.80 to 0.97). RMSEs between the IMC-PGRF and OMC-MGRF models ranged from 44.87%BW to 74.69%BW for the axial compression force, from 7.98%BW to 22.73%BW for the anteroposterior shear force, and from 1.71%BW to 4.06%BW for the mediolateral shear force. When comparing the OMC-PGRF and OMC-MGRF models, the RMSEs for the axial compression, anteroposterior, and mediolateral shear forces ranged from 13.35%BW to 27.15%BW, from 2.38%BW to 5.80%BW, and from 0.23%BW to 0.58%BW, respectively. rRMSEs between the IMC-PGRF and OMC-MGRF models ranged from 22.79% to 112.87% for the axial compression force, from 34.47% to 57.53% for the anteroposterior shear force, and from 50.33% to 126.59% for the mediolateral shear force. The errors between the OMC-MGRF and OMC-PGRF models ranged from 4.72%BW to 40.09%BW for the axial compression force, from 4.38% to 36.36% for the anteroposterior shear force, and from 6.51% to 15.21% for the mediolateral shear force.

Time-series Bland-Altman plots comparing the L4-L5 axial compression forces between the IMC-PGRF and OMC-MGRF models as well as between the OMC-PGRF and OMC-MGRF models for all lifting conditions separately and combined are illustrated in Fig. 6. For all trials combined, the IMC-PGRF model underestimated and the OMC-PGRF model overestimated the L4-L5 axial compression force compared to the OMC-MGRF model (see Table 4).

**5.4 Erector spinae muscle forces**

The erector spinae muscle force showed moderate to excellent correlations between the IMC-PGRF and OMC-MGRF models (see Table 3) for symmetrical and asymmetrical lifting (ICC ranging from 0.74 to 0.94), and moderate to good correlations during the transferring tasks (ICC ranging from 0.64 to 0.78). When comparing the OMC-PGRF and OMC-MGRF models, excellent correlations were found during symmetrical and asymmetrical lifting (ICC ranging from 0.95 to 0.98), while the transferring tasks showed moderate to excellent correlations (ICC ranging from 0.62 to 0.90). RMSE and rRMSE between the IMC-PGRF and OMC-MGRF models ranged from

13.46%BW to 32.52%BW and 11.33% to 47.60%, respectively, across all conditions. OMC-PGRF compared with OMC-MGRF showed RMSEs from 6.16%BW to 13.76%BW, while rRMSEs ranged from 4.72% to 42.90%.

## 6. Discussion

In this study, we evaluated the concurrent validity of an inverse dynamics musculoskeletal model driven by IMC and predicted GRF&Ms to estimate the internal loading of the spine during common lifting and transferring tasks by comparing it to a more traditional model driven by OMC and MGRFs. The main findings were that the IMC-PGRF models showed moderate to excellent correlations (ICC ranging 0.51 to 0.96) and relatively low magnitude differences (rRMSE ranging from 10.55 to 34.14%) compared to the OMC-MGRF models for the L4-L5 axial compression force, erector spinae muscle force and vertical GRFs during all two-handed symmetric and asymmetric lifting trials. However, substantial magnitude differences (rRMSE ranging from 134.1 to 198.80%) were identified for the trunk flexion angles during 6 of the 8 analyzed tasks, which represent the clearest discrepancy between the IMC-PGRF and OMC-MGRF models.

The experimental procedures enabled a direct comparison between measured and predicted vertical GRFs based on IMC and OMC data separately for both the right and left leg. The results showed moderate to excellent correlations for OMC-MGRF versus IMC-PGRF (ICC ranging from 0.51 to 0.96), while excellent correlations were found for OMC-MGRF versus OMC-PGRF (ICC ranging from 0.86 to 0.98). Similarly, RMSE and rRMSE showed lower magnitude differences between the OMC models compared to IMC-PGRF versus OMC-MGRF, indicating that the differences in the models' kinematic inputs and scaling techniques affect the computation of the vertical GRF. Compared to other studies using IMC to estimate the vertical GRF, the present study showed similar accuracy as Faber et al.[10] and Karatsidis et al.[21,22]. In addition, similar results were found for the right and left foot, indicating that the muscle recruitment algorithm was able to distribute the vertical GRFs accurately, despite there being several closed kinematic chains in the analyzed tasks. Direct comparisons of the mediolateral and anteroposterior GRFs, and transversal, sagittal, and frontal GRMs are presented in the supplementary material (Supplementary Fig. 2-5, Table 1-2). Although our approach was similar to that of Karatsidis et al.[22], larger errors were found for the anteroposterior and mediolateral GRFs, as well as the

GRMs. This is likely due to the more complex tasks analyzed in the present study, where the models are moving an object with either one or two hands.

The IMC-PGRF model's estimated L4-L5 axial compression forces were most similar during symmetrical and asymmetrical lifting, while the differences were considerably larger for the transferring tasks (see Table 1). Furthermore, larger RMSEs were observed with increments in load. However, when comparing the relative accuracy between lifts using rRMSE, there seemed to be little influence of weight increments for the symmetrical and asymmetrical lifting tasks, while a trend towards less accurately estimated anteroposterior shear forces was found as a result of the weight increments. The mediolateral shear forces showed low correlations overall and high rRMSEs for IMC-PGRF versus OMC-MGRF. However, the magnitudes of these forces were very low, making the computations more sensitive to noise in the experimental data. This issue was similarly observed in Skals et al.[36], which also showed a clear trend towards higher correlation coefficients with higher signal magnitudes. Hence, we believe that the low signal-to-noise ratio was the predominant reason for the low correlations and high rRMSEs for the mediolateral shear forces, and we do not expect this to be an issue when analyzing mediolateral shear forces of a meaningful magnitude.

Typically, mediolateral shear forces are less crucial for the traditional ergonomic evaluation of manual materials handling, as either the axial compression[29,41] or anteroposterior shear force[16] are used as the main parameters to determine critical low back loading. However, many occupational lifts are highly asymmetrical, making accurate mediolateral shear forces a potentially valuable indicator of the risk of spinal injury during occupational lifting.

As indicated in Fig. 6, the median and percentile values for the L4-L5 axial compression force of the IMC-PGRF models are less accurate than for the OMC-PGRF models compared to OMC-MGRF (see Table 4). Furthermore, the IMC-PGRF models underestimated the L4-L5 axial compression forces overall, but similar trends were identified, indicated by the good to excellent correlations for the symmetrical and asymmetrical lifting conditions (see Table 1). Based on these results, we believe that the IMC-PGRF model can be used to get a reasonable estimate of L4-L5 axial compression forces under dynamic conditions in the field, which has previously not been possible. Even more important is that the IMC-PGRF model can be used as an ergonomic tool to

compare the relative L4-L5 axial compression force between different occupational lifting situations at the workplace.

The IMC-PGRF versus OMC-MGRF comparison showed higher correlations and lower rRMSE during symmetrical and asymmetrical lifting than during the transferring tasks (Table 3) for the erector spinae muscle force. Similar to the estimated anteroposterior shear force, the estimated erector spinae muscle force showed a trend of increasing difference with weight increments for symmetrical and asymmetrical lifting. Because the IMC and OMC models applied different methods for scaling the body segments, differences in muscle moment arms and errors in the predicted GRF&Ms could explain some of the differences between the IMC-PGRF and OMC-MGRF models. Another contributing factor to the differences in the erector spinae muscle force, and thereby also the L4-L5 JRFs, are the differences in the pelvis-thorax flexion angle between the IMC and OMC models (see Fig. 3 and 4). During symmetrical and asymmetrical lifting, the pelvis-thorax flexion angle showed RMSEs ranging from 12.43 to 17.53 degrees, while for the transferring tasks, RMSEs ranged from 6.86 to 7.34 degrees. These kinematic errors were generally larger than those previously reported[22,23]. However, these studies analyzed different movements and only compared joint angles for the lower extremities, so a direct comparison is not possible. We believe that the relatively large differences found in the present study for the pelvis-thorax flexion angle are likely caused by 2 main issues. First, only 4 IMUs (one placed on the pelvis, the sternum and one on each scapula) are used to determine the relative angle between pelvis and thorax for the IMC system compared to 10 reflective markers (4 on the pelvis, 2 on the spine and the shoulders, and 1 on the sternum and between the clavicles) for the OMC system. Therefore, it is reasonable to assume that the IMC system is not able to provide similar accuracy to the OMC system, particularly during movements involving large trunk flexion. Second, inaccurate placement of the pelvis IMU during measurements: in the present study, the male subjects (9 out of 13) only wore tights to avoid introducing additional soft tissue artefacts, as the markers had to be placed on top of the fabric of the customized t-shirt associated with the IMC system. However, placing the pelvis IMU on top of the sacrum was difficult due to its complex geometry without one prominent bony attachment point, and furthermore, it typically corresponded with the subjects' waistband. Therefore, the IMU may have been placed too

superiorly, so it spanned the top of the sacrum, almost reaching the iliac crest, which likely decreased the system's ability to measure the relative angle between pelvis and thorax. In addition, keeping the pelvis IMU in place using the accompanying straps can be challenging during large trunk flexions, and it needs to be continuously corrected during data collection to avoid errors. Although not presented here, the IMC ankle, knee, hip, and shoulder angles were more accurate, similar to the results of other studies evaluating the accuracy of IMUs[22,23], indicating that the placement and difficulty of maintaining the position of the pelvis IMU could have contributed to the inaccuracies reported in the present study. When viewing the other results, the differences in the pelvis-thorax flexion angles only led to relatively small differences in the estimation of L4-L5 axial compression, erector spinae muscle and vertical GRFs, but have likely contributed greatly to the observed differences for some of the other analyzed variables, especially the anteroposterior shear forces in more bended positions. Specific ways to improve the IMC-PGRF models estimation of the pelvis-thorax angle are hard to determine and will likely require development efforts from the manufactures of the IMC system. One suggestion could be to use the more detailed musculoskeletal model instead of the kinematic model associated with the IMC system to reconstruct the motion data from the IMUs during the sensor fusion procedure. This would also avoid introducing the stick figure with virtual markers to reconstruct the motion data from the IMC system, which could also be associated with inaccuracies. However, the methodology for doing this does not currently exists and will have to be developed.

The present work was associated with several limitations. First, although the OMC-MGRF was assumed a silver standard, it is well-known that the magnitudes of estimated spinal loadings are less accurate during large lateral bending movements[4] and sensitive to other model parameters, such as spine rhythm, intra-abdominal pressure, joint stiffness, musculature, and ligaments[3,15,17]. Therefore, it is important to note that the silver standard in this case also entail uncertainties. Second, measurements of human motion are prone to soft tissue artefacts with most research showing the largest influence during movements in the frontal and transverse planes[25]. However, the present study investigated movements performed at a slow pace and with no sudden accelerations, reducing the influence of soft tissue artefacts to some extent. Third, the OMC models were scaled according to the attachment of reflective markers, while the IMC models

were scaled based on manually measured segment dimensions, which introduced slight differences in segment lengths. Fourth, to reduce sliding of the reflective markers that had to be placed on top of the customized t-shirt associated with the IMC system, we asked the participants, if they felt comfortable doing so, to be shirtless. However, the female participants felt more comfortable with the shirt on during testing and were allowed to wear it. We do not believe that this decision had any notable effect on the IMC measurements, but may have introduced slightly larger tracking errors for the reflective markers placed on the sternum, clavicular, left and right acromion, C7 and T12 for the female subjects compared to the male subjects. Fifth, the kinematics of the box lifted during the experiment was not measured using the IMC system, but rather driven by the positions and rotations of the hands. Although we expect this to have minor influence on the computations of spinal loading, it would have been more appropriate to use additional IMUs to determine the kinematics of the box. Sixth, the forces at the hand-box coupling were not measured, but modelled with additional contact elements. Measured grip forces could potentially improve the accuracy of the models' kinetic computations above the thorax, e.g. the shoulder and elbow JRFs, which are also relevant indicators of physical workload during manual materials handling. Finally, the thoracic part has been modelled as a rigid segment. However, Ignasiak et al.[20] showed that lumbar spine models with a rigid thorax definition can be used to estimate the loading at the lower lumbar levels.

In summary, the accuracy of a musculoskeletal model based on IMC and PGRF for computing L4-L5 JRFs, erector spinae muscle forces, GRFs and trunk kinematics was evaluated against a model based on OMC and MGRF. The analysis showed that the IMC-PGRF model can be used to estimate musculoskeletal loading during standard manual materials handling tasks under dynamic conditions, such as symmetrical and asymmetrical lifting with varying weight, with reasonable accuracy. Based on these results, we believe that this methodology can be highly useful for estimating relative L4-L5 axial compression forces under dynamic conditions during manual materials handling in the field.

## Conflict of interest

Mark de Zee is co-founder of the company AnyBody Technology A/S that owns and sells the AnyBody Modeling System, which was used for the simulations. Mark de Zee is also a minority shareholder in the company.

## 7. Acknowledgments

This work was supported by the Independent Research Fund Denmark under grant no. DFF-7026-00099 to Sebastian Skals.

## Appendix

Supplementary data for this article can be found online.

## 8. References

1. Andersen, M. S., M. Damsgaard, B. MacWilliams, and J. Rasmussen. A computationally efficient optimisation-based method for parameter identification of kinematically determinate and over-determinate biomechanical systems. *Comput. Methods Biomech. Biomed. Engin.* 13:171–183, 2010.
2. Andersen, M. S., M. Damsgaard, and J. Rasmussen. Kinematic analysis of over-determinate biomechanical systems. *Comput. Methods Biomech. Biomed. Engin.* 12:371–384, 2009.
3. Arshad, R., T. Zander, M. Dreischarf, and H. Schmidt. Influence of lumbar spine rhythms and intra-abdominal pressure on spinal loads and trunk muscle forces during upper body inclination. *Med. Eng. Phys.* 38:333–338, 2016.
4. Bassani, T., E. Stucovitz, Z. Qian, M. Briguglio, and F. Galbusera. Validation of the AnyBody full body musculoskeletal model in computing lumbar spine loads at L4L5 level. *J. Biomech.* 58:89–96, 2017.
5. Bland, M. J., and G. D. Altman. Measuring agreement in method comparison studies. *Stat. Methods Med. Res.* 8:135–160, 1999.
6. Carbone, V., R. Fluit, P. Pellikaan, M. M. van der Krogt, D. Janssen, M. Damsgaard, L. Vigneron, T. Feilkas, H. F. J. M. Koopman, and N. Verdonschot. TLEM 2.0 - A comprehensive musculoskeletal geometry dataset for subject-specific modeling of lower extremity. *J. Biomech.* 48:734–741, 2015.
7. Deyo, R. A., and J. N. Weinstein. Low Back Pain. *N. Engl. J. Med.* 344:363–370, 2001.
8. Van Dieën, J. H. H., H. Weinans, and H. M. M. Toussaint. Fractures of the lumbar vertebral endplate in the etiology of low back pain: a hypothesis on the causative role of spinal compression in aspecific low back pain. *Med. Hypotheses* 53:246–252, 1999.
9. Dreischarf, M., A. Shirazi-Adl, N. Arjmand, A. Rohlmann, and H. Schmidt. Estimation of loads on human lumbar spine: A review of in vivo and computational model studies. *J. Biomech.* 49:833–845, 2016.
10. Faber, G. S., C. C. Chang, I. Kingma, J. T. Dennerlein, and J. H. van Dieën. Estimating 3D L5/S1 moments and ground reaction forces during trunk bending using a full-body ambulatory inertial motion capture system. *J. Biomech.* 49:904–912, 2016.
11. Faber, G. S., I. Kingma, N. Delleman, and J. van Dieën. Effect of ship motion on spinal loading during manual lifting. *Ergonomics* 51:1426–1440, 2008.
12. Filippeschi, A., N. Schmitz, M. Miezal, G. Bleser, E. Ruffaldi, and D. Stricker. Survey of Motion Tracking Methods Based on Inertial Sensors: A Focus on Upper Limb Human Motion. *Sensors* 17:1257, 2017.
13. Fluit, R., M. S. Andersen, S. Kolk, N. Verdonschot, and H. F. J. M. J. M. Koopman. Prediction of ground reaction

forces and moments during various activities of daily living. *J. Biomech.* 47:2321–2329, 2014.

14. Frankenfield, D. C., W. A. Rowe, R. N. Cooney, J. S. Smith, and D. Becker. Limits of body mass index to detect obesity and predict body composition. *Nutrition* 17:26–30, 2001.
15. Galibarov, P. E., S. Dendorfer, and J. Rasmussen. Two Computational Models of the Lumbar Spine: Comparison and Validation. *ORS Annu Meet* 2011, 2011.
16. Gallagher, S., and W. S. Marras. Tolerance of the lumbar spine to shear: A review and recommended exposure limits. *Clin. Biomech.* 27:973–978, 2012.
17. Han, K. S., T. Zander, W. R. Taylor, and A. Rohlmann. An enhanced and validated generic thoraco-lumbar spine model for prediction of muscle forces. *Med. Eng. Phys.* 34:709–716, 2012.
18. Hansen, L., M. De Zee, J. Rasmussen, T. B. Andersen, C. Wong, and E. B. Simonsen. Anatomy and biomechanics of the back muscles in the lumbar spine with reference to biomechanical modeling. *Spine (Phila. Pa. 1976).* 31:1888–1899, 2006.
19. Van der Helm, F. C. T., H. E. J. Veeger, G. M. Pronk, L. H. V. Van der Woude, and R. H. Rozendal. Geometry parameters for musculoskeletal modelling of the shoulder system. *J. Biomech.* 25:129–144, 1992.
20. Ignasiak, D., S. J. Ferguson, and N. Arjmand. A rigid thorax assumption affects model loading predictions at the upper but not lower lumbar levels. *J. Biomech.* 49:3074–3078, 2016.
21. Karatsidis, A., G. Bellusci, H. Schepers, M. de Zee, M. Andersen, and P. Veltink. Estimation of Ground Reaction Forces and Moments During Gait Using Only Inertial Motion Capture. *Sensors* 17:75, 2016.
22. Karatsidis, A., M. Jung, H. M. Schepers, G. Bellusci, M. de Zee, P. H. Veltink, and M. S. Andersen. Musculoskeletal model-based inverse dynamic analysis under ambulatory conditions using inertial motion capture. *Med. Eng. Phys.* 57:1–31, 2019.
23. Koning, B. H. W., M. M. van der Krogt, C. T. M. Baten, and B. F. J. M. Koopman. Driving a musculoskeletal model with inertial and magnetic measurement units. *Comput. Methods Biomech. Biomed. Engin.* 18:1003–1013, 2015.
24. Koo, T. K., and M. Y. Li. A Guideline of Selecting and Reporting Intraclass Correlation Coefficients for Reliability Research. *J. Chiropr. Med.* 15:155–63, 2016.
25. Leardini, A., A. Chiari, U. Della Croce, and A. Cappozzo. Human movement analysis using stereophotogrammetry Part 3. Soft tissue artifact assessment and compensation. *Gait Posture* 21:212–225, 2005.
26. McLaughlin, P. Testing agreement between a new method and the gold standard-How do we test? *J. Biomech.* 46:2757–2760, 2013.
27. Meldrum, D., C. Shouldice, R. Conroy, K. Jones, and M. Forward. Test-retest reliability of three dimensional gait analysis: Including a novel approach to visualising agreement of gait cycle waveforms with Bland and Altman plots. *Gait Posture* 39:265–271, 2014.
28. Moisio, K. C., D. R. Sumner, S. Shott, and D. E. Hurwitz. Normalization of joint moments during gait: A comparison of two techniques. *J. Biomech.* 36:599–603, 2003.
29. NIOSH. Work Practices Guide for Manual Lifting. Washington, DC, US: 1981.
30. Rajaee, M. A., N. Arjmand, A. Shirazi-Adl, A. Plamondon, and H. Schmidt. Comparative evaluation of six quantitative lifting tools to estimate spine loads during static activities. *Appl. Ergon.* 48:22–32, 2015.
31. Rasmussen, J., M. de Zee, and S. Carbes. Validation of a biomechanical model fo the lumbar spine. , 2009.
32. Rasmussen, J., M. De Zee, M. Damsgaard, S. Tørholm Christensen, C. Marek, and K. Siebertz. A general method for scaling musculo-skeletal models. *2005 Int. Symp. Comput. Simul. Biomech.* 3, 2005.
33. Ren, L., R. K. Jones, and D. Howard. Whole body inverse dynamics over a complete gait cycle based only on measured kinematics. *J. Biomech.* 41:2750–2759, 2008.
34. Roetenberg, D., H. J. Luinge, and P. Slycke. Xsens MVN : Full 6DOF Human Motion Tracking Using Miniature Inertial Sensors. Enschede, The Netherlands: 2013.
35. Shrout, P. E., and J. L. Fleiss. Intraclass correlations: Uses in assessing rater reliability. *Psychol. Bull.* 86:420–428, 1979.
36. Skals, S., M. K. Jung, M. Damsgaard, and M. S. Andersen. Prediction of ground reaction forces and moments

during sports-related movements. *Multibody Syst. Dyn.* 39:175–195, 2017.

37. Skals, S., K. P. Rasmussen, K. M. Bendtsen, J. Yang, and M. S. Andersen. A musculoskeletal model driven by dual Microsoft Kinect Sensor data. *Multibody Syst. Dyn.* 41:297–316, 2017.
38. Veeger, H. E. J., F. C. T. Van Der Helm, L. H. V. Van Der Woude, G. M. Pronk, and R. H. Rozendal. Inertia and Muscle-Contraction Parameters for Musculoskeletal Modeling of the Shoulder Mechanism. *J. Biomech.* 24:615-, 1991.
39. Veeger, H. E. J., B. Yu, K. N. An, and R. H. Rozendal. Parameters for modeling the upper extremity. *J. Biomech.* 30:647–652, 1997.
40. Veltink, P. H., C. Liedtke, E. Droog, and H. Van Der Kooij. Ambulatory measurement of ground reaction forces. *IEEE Trans. Neural Syst. Rehabil. Eng.* 13:423–427, 2005.
41. Waters, T. R., V. Putz-Anderson, A. Garg, and L. J. Fine. Revised NIOSH equation for the design and evaluation of manual lifting tasks. *Ergonomics* 36:749–776, 1993.
42. Wilke, H.-J., P. Neef, B. Hinz, H. Seidel, and L. Claes. Intradiscal pressure together with anthropometric data – a data set for the validation of models. *Clin. Biomech.* 16, Supple:S111--S126, 2001.
43. Winter, D. A. Biomechanics and Motor Control of Human Movement. Hoboken, N.J. : John Wiley, 2009.
44. de Zee, M., L. Hansen, C. Wong, J. Rasmussen, and E. B. Simonsen. A generic detailed rigid-body lumbar spine model. *J. Biomech.* 40:1219–1227, 2007.

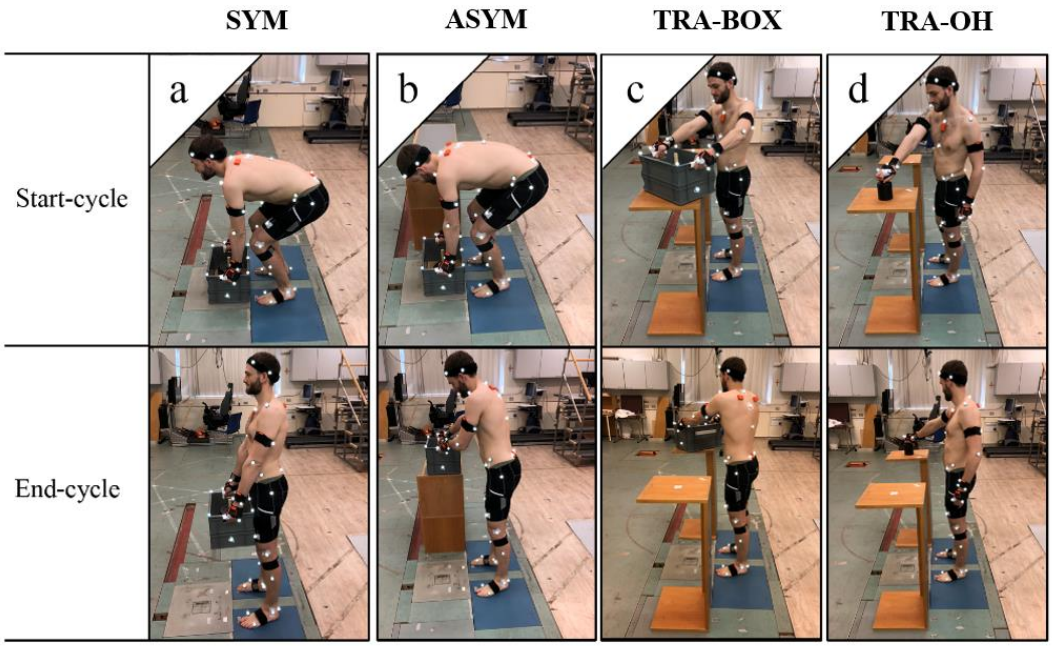


**Fig. 1:** a: Symmetrical lifting (SYM) involves lifting a 5, 10, 15, and 20 kg box from the floor to an upright position. b: Asymmetrical lifting (ASYM) involves lifting a 5 and 10 kg box from the floor and placing it on a table to the subject's right side. c: Two-handed transferring (TRA-BOX) involves transferring a 10 kg box from one table to another. d: One-handed transferring (TRA-OH) involves transferring a 5 kg weight with one hand from one table to another.

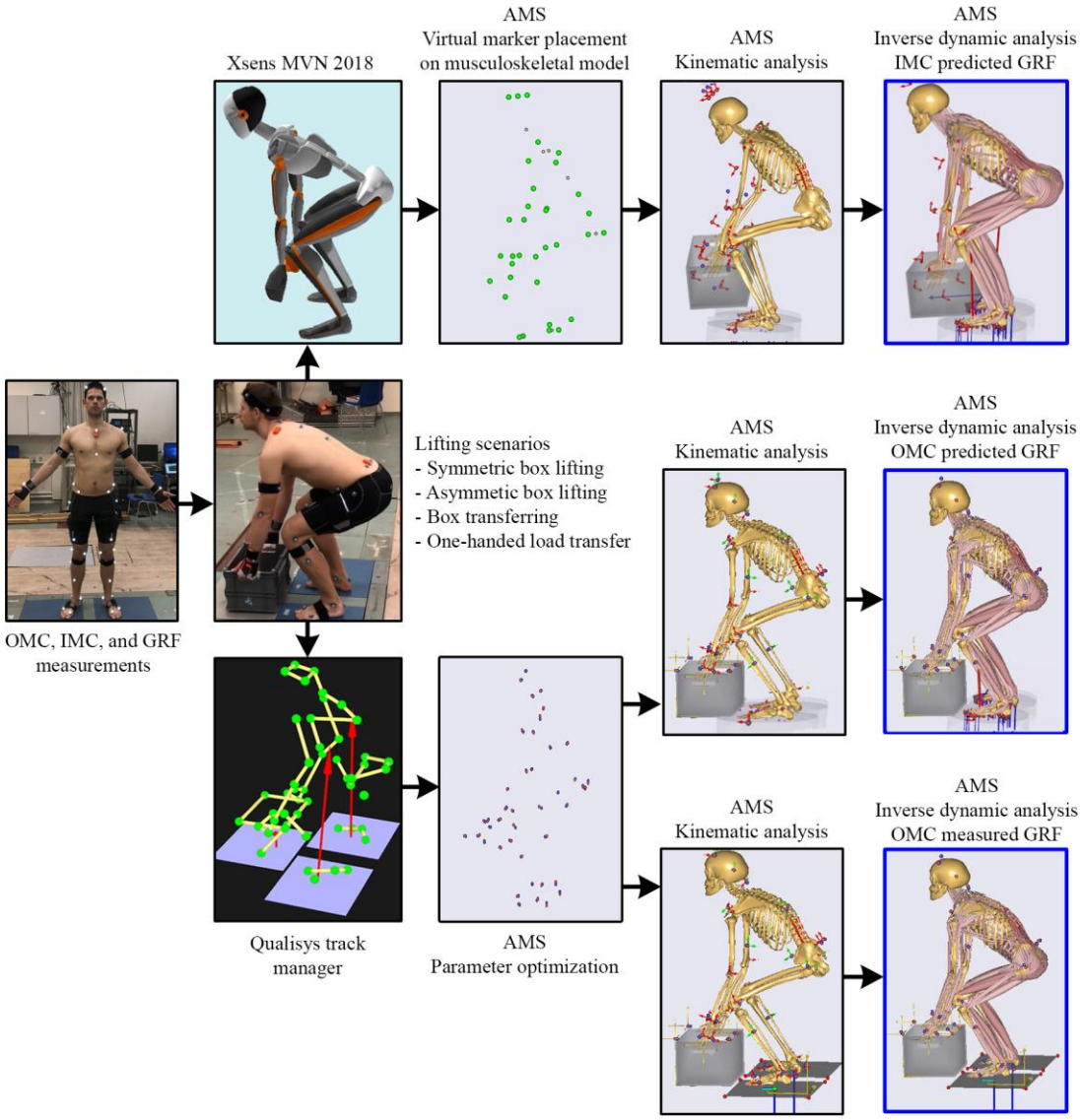


**Fig. 2:** Flowchart illustrating the development of the three musculoskeletal models in the AnyBody Modeling System (AMS): 1) inertial motion capture with predicted ground reaction forces (IMC-PGRF), 2) optical motion capture with predicted ground reaction forces (OMC-PGRF), and 3) optical motion capture with measured ground reaction forces (OMC-MGRF).

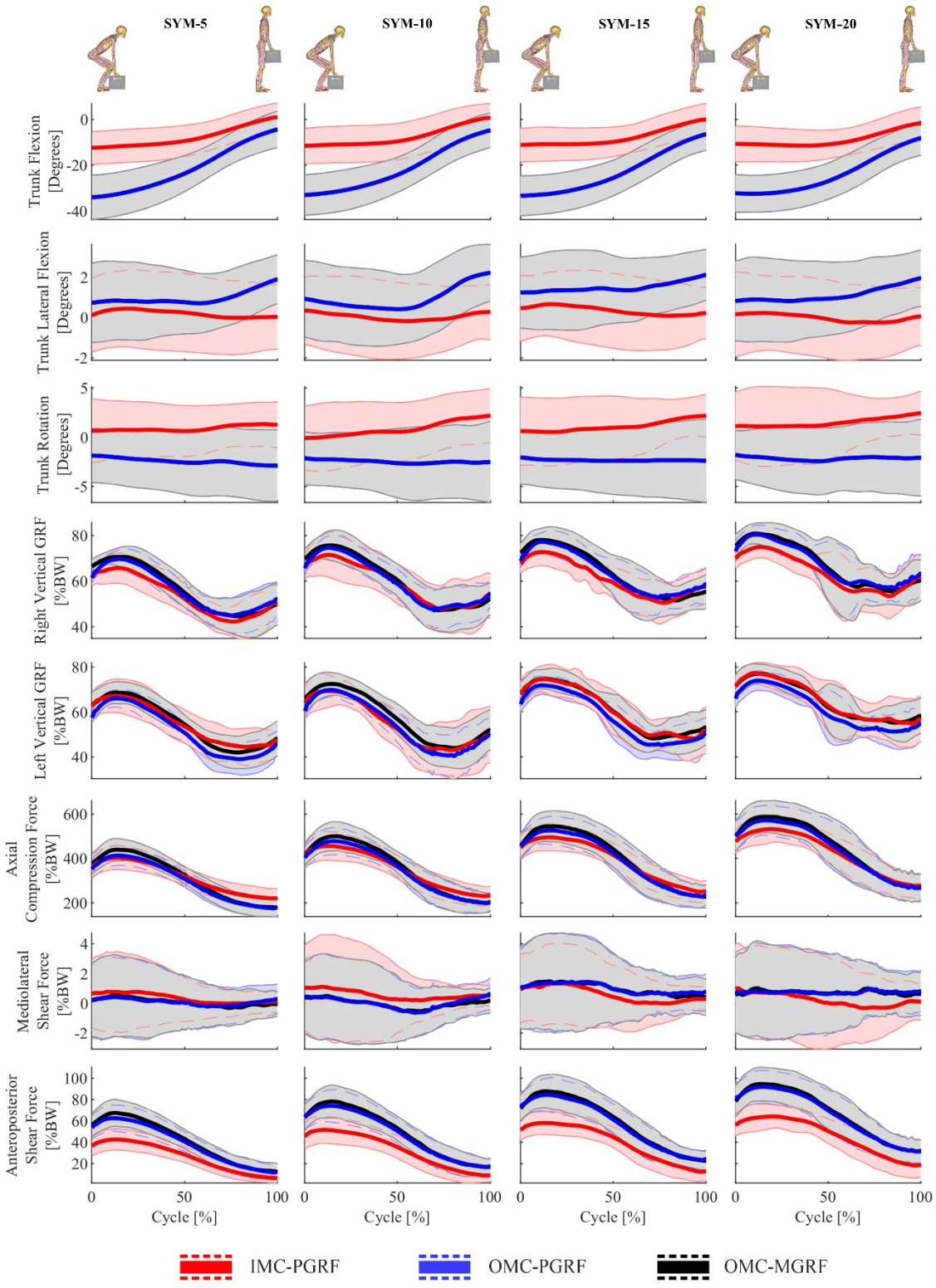


**Fig. 3:** Average trunk angles, vertical ground reaction forces (GRFs) for the right and left foot, and joint reaction forces (JRFs) (mean (line) ± SD (shaded area)) during symmetrical lifting (SYM) with 5, 10, 15 and 20 kg for the models driven by inertial motion capture with predicted ground reaction forces (IMC-PGRF), illustrated in red, 2) optical motion capture with predicted ground

reaction forces (OMC-PGRF), illustrated in blue, and 3) optical motion capture with measured ground reaction forces (OMC-MGRF), illustrated in black.

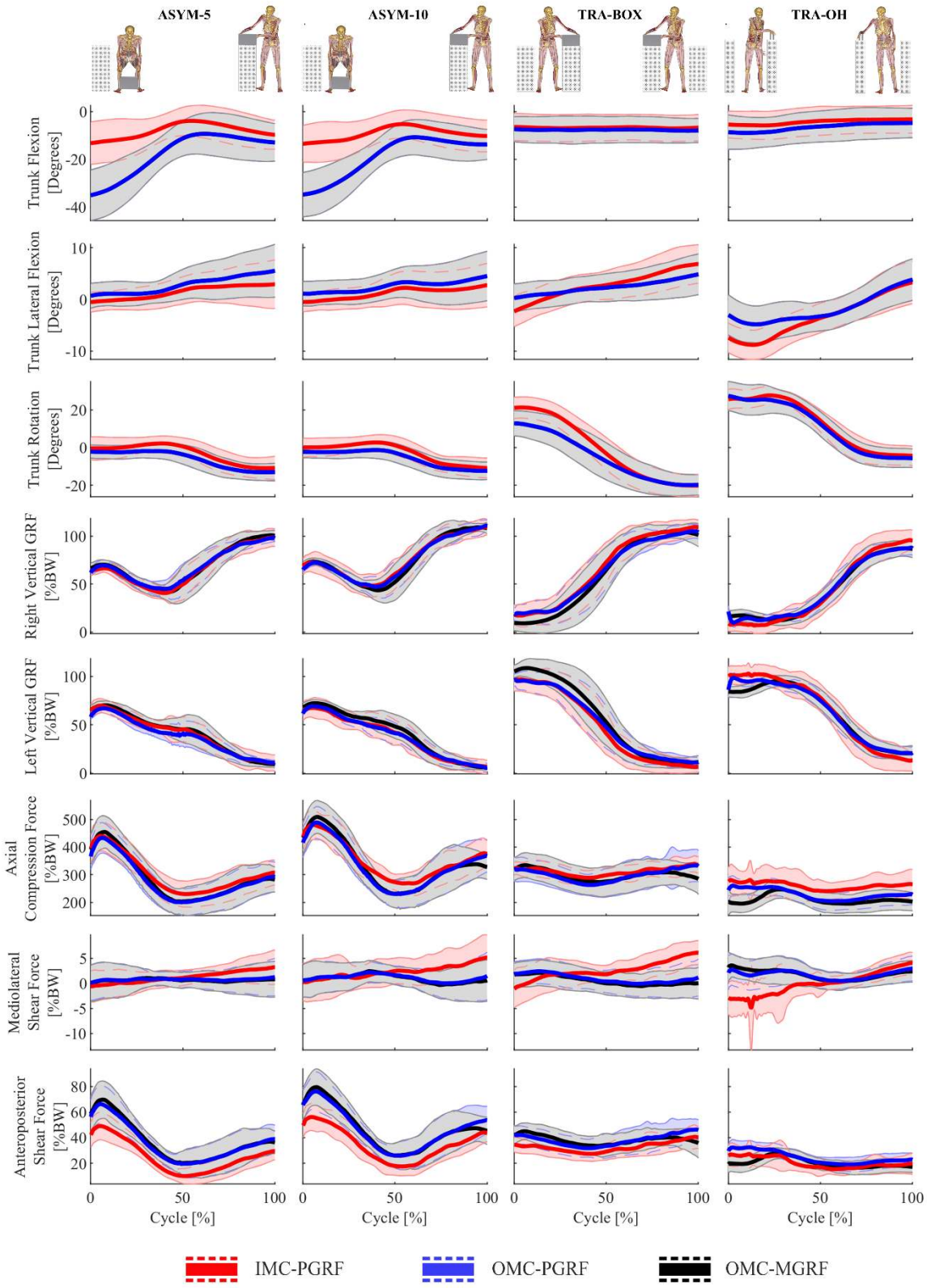


**Fig. 4:** Average trunk angles, vertical ground reaction force (GRF) for the right and left foot, and joint reaction forces (JRFs) (mean (line) ± SD (shaded area)) during asymmetrical lifting (ASYM) with 5 and 10 kg as well as one- (TRA-OH) and two-handed (TRA-

BOX) transferring for the models driven by inertial motion capture with predicted ground reaction forces (IMC-PGRF), illustrated in red, 2) optical motion capture with predicted ground reaction forces (OMC-PGRF), illustrated in blue, and 3) optical motion capture with measured ground reaction forces (OMC-MGRF), illustrated in black.

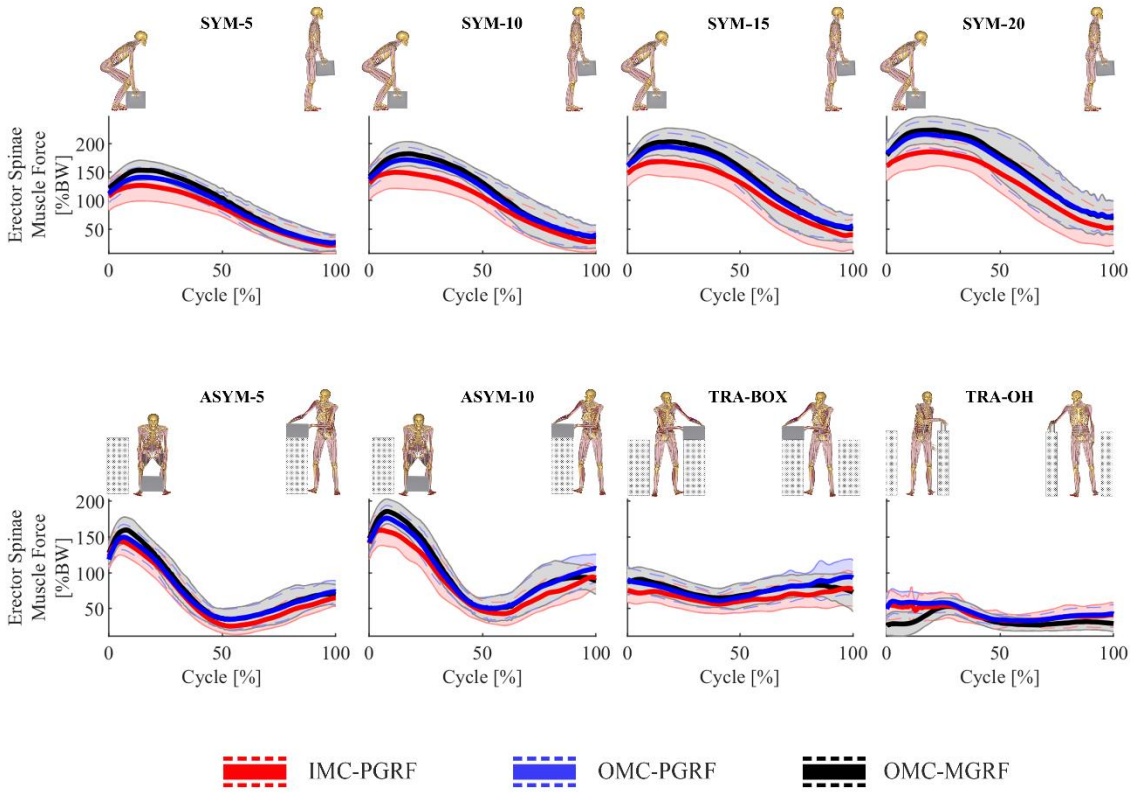


**Fig. 5:** Average erector spinae muscle force (mean (line) ± SD (shaded area)) during symmetrical (SYM) and asymmetrical (ASYM) lifting as well as one- (TRA-OH) and two-handed (TRA-BOX) transferring for the models driven by inertial motion capture with predicted ground reaction forces (IMC-PGRF), illustrated in red, 2) optical motion capture with predicted ground reaction forces (OMC-PGRF), illustrated in blue, and 3) optical motion capture with measured ground reaction forces (OMC-MGRF), illustrated in black.

(a)

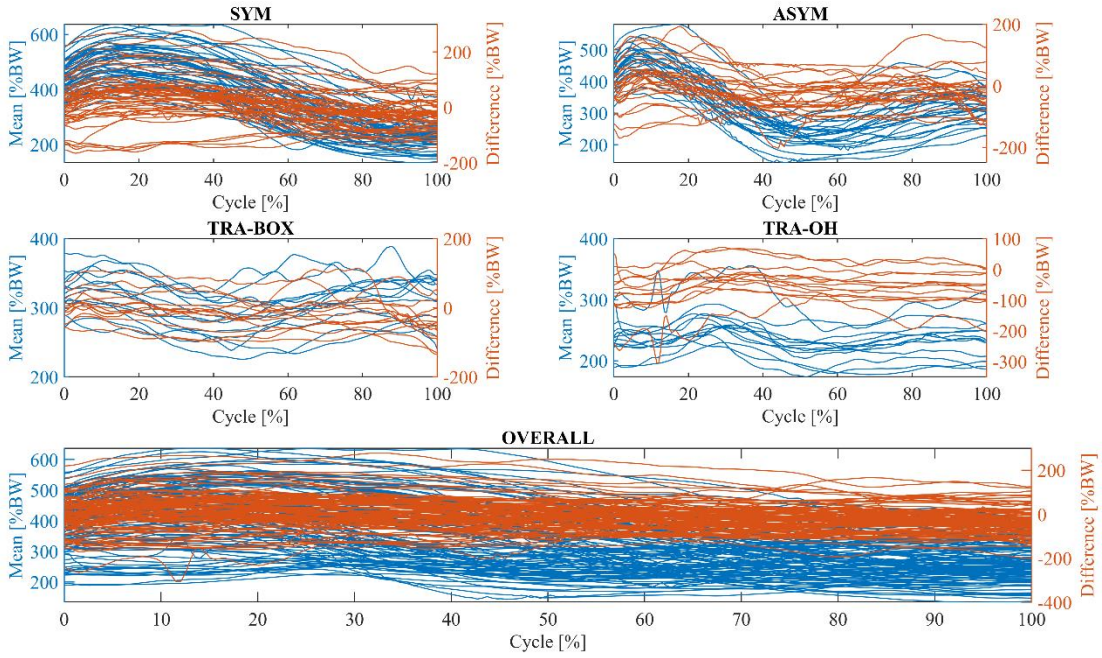


(b)

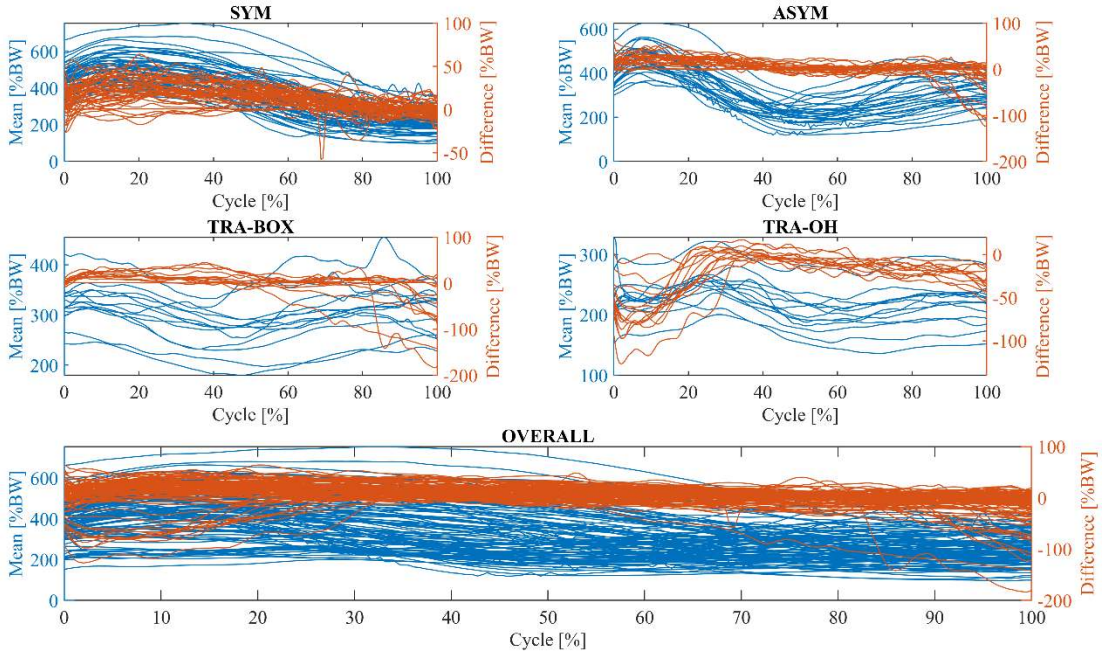


**Fig. 6:** Bland Altman plots illustrating the normalized time-series data for the mean and difference of the L4-L5 axial compression force (%BW) for (a) optical motion capture with measured ground reaction forces (OMC-MGRF) versus inertial motion capture with predicted ground reaction forces (IMC-PGRF) and (b) optical motion capture with measured ground reaction forces (OMC-MGRF) versus optical motion capture with predicted ground reaction forces (OMC-PGRF). The blue lines represent the mean and the orange lines the difference. Symmetrical lifting (SYM), asymmetrical lifting (ASYM), one- (TRA-OH) and two-handed (TRA-

BOX) transferring are presented separately (first and second row) and combined for all lifting conditions (third row). Please note the difference in the values of the y-axis between (a) and (b).

**Table 1:** Inertial motion capture with predicted ground reaction forces (IMC-PGRF) versus optical motion capture with measured ground reaction forces (OMC-MGRF) for symmetrical lifting (SYM) with 5, 10, 15 and 20 kg, asymmetrical lifting (ASYM) with 5 and 10 kg as well as one- (TRA-OH) and two-handed transferring (TRA-BOX). ICC = intraclass correlation coefficient (mean), RMSE = root mean square error (%BW) (mean ± SD), and rRMSE = relative root mean square error (%) (mean ± SD). Results are presented for trunk flexion, lateral flexion and rotation, vertical GRF for the right and left foot, axial compression force, mediolateral and anteroposterior shear force.

| | SYM-5 | SYM-10 | SYM-15 | SYM-20 | ASYM-5 | ASYM-10 | TRA-BOX | TRA-OH |
|---|---|---|---|---|---|---|---|---|
| | | | | ICC | | | | |
| Trunk flexion | 0.34 | 0.41 | 0.34 | 0.31 | 0.31 | 0.28 | 0.20 | 0.21 |
| Trunk lateral flexion | -0.01 | 0.16 | -0.08 | 0.10 | 0.24 | 0.19 | 0.28 | 0.41 |
| Trunk rotation | 0.07 | 0.09 | 0.08 | 0.01 | 0.51 | 0.47 | 0.79 | 0.83 |
| Right vertical GRF | 0.64 | 0.69 | 0.71 | 0.66 | 0.92 | 0.94 | 0.96 | 0.94 |
| Left vertical GRF | 0.74 | 0.77 | 0.69 | 0.51 | 0.93 | 0.96 | 0.96 | 0.92 |
| Axial compression force | 0.88 | 0.90 | 0.91 | 0.85 | 0.85 | 0.92 | 0.57 | 0.16 |
| Mediolateral shear force | 0.01 | 0.43 | 0.04 | 0.09 | 0.37 | 0.51 | 0.23 | 0.04 |
| Anteroposterior shear force | 0.65 | 0.77 | 0.79 | 0.73 | 0.78 | 0.79 | 0.78 | 0.74 |
| | | | | RMSE | | | | |
| Trunk flexion | 15.23 (6.82) | 15.39 (7.03) | 16.38 (8.06) | 16.54 (8.38) | 12.43 (6.41) | 12.75 (6.77) | 6.86 (4.41) | 7.34 (6.54) |
| Trunk lateral flexion | 1.80 (0.87) | 2.19 (1.04) | 2.16 (1.15) | 2.12 (1.23) | 2.67 (0.94) | 2.79 (1.49) | 2.46 (1.35) | 2.89 (1.51) |
| Trunk rotation | 4.58 (3.52) | 4.76 (3.42) | 4.92 (3.36) | 5.02 (3.04) | 5.22 (4.16) | 5.35 (3.99) | 7.75 (3.25) | 5.06 (3.15) |
| Right vertical GRF | 6.28 (3.43) | 7.47 (3.18) | 6.26 (2.76) | 6.91 (2.97) | 6.87 (2.59) | 10.09 (3.50) | 11.58 (6.12) | 9.33 (2.67) |
| Left vertical GRF | 5.57 (2.61) | 6.64 (2.97) | 5.06 (2.14) | 5.49 (2.36) | 6.53 (1.94) | 9.57 (4.83) | 12.14 (6.81) | 11.23 (3.31) |
| Axial compression force | 58.02 (33.7) | 66.91 (33.9) | 68.42 (49.2) | 74.69 (57.4) | 50.05 (29.0) | 57.17 (31.1) | 44.87 (24.4) | 63.52 (39.4) |
| Mediolateral shear force | 1.71 (0.67) | 2.43 (1.52) | 2.62 (1.05) | 2.66 (1.55) | 2.70 (1.38) | 4.03 (1.76) | 3.79 (1.28) | 4.06 (2.49) |
| Anteroposterior shear force | 16.81 (8.39) | 18.93 (10.7) | 20.87 (14.2) | 22.73 (16.4) | 13.40 (7.58) | 14.49 (8.30) | 8.37 (4.27) | 7.98 (5.16) |
| | | | | rRMSE | | | | |
| Trunk flexion | 134.1 (109.8) | 169.7 (233.9) | 186.4 (217.1) | 198.0 (182.9) | 129.27 (91.6) | 187.1 (207.7) | 246.5 (219.0) | 203.4 (175.4) |
| Trunk lateral flexion | 145.4 (132.7) | 180.9 (132.2) | 150.4 (113.0) | 129.92 (75.8) | 70.62 (53.09) | 81.69 (75.46) | 31.30 (20.53) | 40.66 (65.70) |
| Trunk rotation | 138.4 (104.0) | 165.1 (142.4) | 203.6 (189.5) | 229.3 (211.0) | 36.92 (32.20) | 36.17 (26.97) | 18.80 (7.08) | 16.03 (11.08) |
| Right vertical GRF | 31.92 (35.41) | 28.82 (20.88) | 25.87 (22.01) | 34.14 (42.03) | 10.94 (4.17) | 14.73 (5.38) | 12.33 (6.69) | 10.29 (3.16) |
| Left vertical GRF | 20.47 (11.61) | 21.40 (9.49) | 15.00 (6.59) | 19.35 (9.47) | 10.55 (2.45) | 15.96 (10.95) | 13.12 (7.45) | 12.07 (3.24) |
| Axial compression force | 33.91 (26.82) | 28.72 (12.24) | 26.46 (17.89) | 27.84 (20.45) | 22.79 (12.06) | 24.86 (14.54) | 67.13 (34.01) | 112.87 (61.0) |
| Mediolateral shear force | 126.59 (87.0) | 78.53 (38.16) | 120.48 (70.8) | 97.27 (66.20) | 57.30 (26.58) | 63.22 (27.19) | 50.33 (33.74) | 61.64 (71.73) |

| | | | | | | | | |
|---|---|---|---|---|---|---|---|---|
| Anteroposterior shear force | 49.07 (28.32) | 46.17 (29.38) | 46.60 (36.15) | 49.58 (37.93) | 34.47 (22.13) | 36.58 (28.94) | 56.64 (38.36) | 57.53 (37.68) |

**Table 2:** Optical motion capture with predicted ground reaction forces (OMC-PGRF) versus optical motion capture with measured ground reaction forces (OMC-MGRF) for symmetrical lifting (SYM) with 5, 10, 15 and 20 kg, asymmetrical lifting (ASYM) with 5 and 10 kg as well as one- (TRA-OH) and two-handed transferring (TRA-BOX). ICC = intraclass correlation coefficient (mean), RMSE = root mean square error (%BW) (mean ± SD), and rRMSE = relative root mean square error (%) (mean ± SD). Results are presented for trunk flexion, lateral flexion and rotation, vertical GRF for the right and left foot, axial compression force, mediolateral and anteroposterior shear force, and erector spinae muscle force.

| | SYM-5 | SYM-10 | SYM-15 | SYM-20 | ASYM-5 | ASYM-10 | TRA-BOX | TRA-OH |
|---|---|---|---|---|---|---|---|---|
| | | | | ICC | | | | |
| Trunk flexion | - | - | - | - | - | - | - | - |
| Trunk lateral flexion | - | - | - | - | - | - | - | - |
| Trunk rotation | - | - | - | - | - | - | - | - |
| Right vertical GRF | 0.96 | 0.97 | 0.97 | 0.96 | 0.98 | 0.98 | 0.97 | 0.96 |
| Left vertical GRF | 0.96 | 0.95 | 0.95 | 0.86 | 0.96 | 0.98 | 0.97 | 0.96 |
| Axial compression force | 0.96 | 0.97 | 0.98 | 0.98 | 0.98 | 0.98 | 0.80 | 0.96 |
| Mediolateral shear force | 0.91 | 0.97 | 0.91 | 1.00 | 0.95 | 0.99 | 0.92 | 0.91 |
| Anteroposterior shear force | 0.97 | 0.98 | 0.98 | 0.98 | 0.98 | 0.98 | 0.83 | 0.97 |
| | | | | RMSE | | | | |
| Trunk flexion | - | - | - | - | - | - | - | - |
| Trunk lateral flexion | - | - | - | - | - | - | - | - |
| Trunk rotation | - | - | - | - | - | - | - | - |
| Right vertical GRF | 2.30 (0.59) | 2.57 (0.93) | 2.83 (1.38) | 2.54 (0.77) | 4.17 (0.89) | 4.81 (1.12) | 8.37 (2.31) | 3.78 (0.66) |
| Left vertical GRF | 3.65 (1.24) | 3.86 (1.35) | 3.98 (1.42) | 4.16 (1.14) | 5.02 (1.02) | 5.44 (1.00) | 8.73 (1.57) | 5.48 (0.95) |
| Axial compression force | 18.72 (9.06) | 17.19 (7.97) | 16.67 (9.20) | 15.54 (7.80) | 13.35 (6.52) | 18.26 (10.7) | 22.18 (20.0) | 27.15 (14.1) |
| Mediolateral shear force | 0.23 (0.11) | 0.24 (0.14) | 0.23 (0.15) | 0.24 (0.14) | 0.26 (0.13) | 0.38 (0.23) | 0.57 (0.54) | 0.58 (0.35) |
| Anteroposterior shear force | 3.12 (1.83) | 2.95 (1.62) | 3.04 (1.83) | 2.86 (1.52) | 2.38 (1.19) | 3.47 (2.15) | 4.52 (3.87) | 5.80 (3.03) |
| | | | | rRMSE | | | | |
| Trunk flexion | - | - | - | - | - | - | - | - |
| Trunk lateral flexion | - | - | - | - | - | - | - | - |
| Trunk rotation | - | - | - | - | - | - | - | - |
| Right vertical GRF | 7.96 (1.63) | 8.28 (2.91) | 8.67 (3.01) | 8.34 (2.47) | 7.01 (1.60) | 6.81 (1.31) | 9.23 (2.51) | 4.72 (0.91) |
| Left vertical GRF | 12.68 (5.69) | 12.22 (5.98) | 13.15 (7.27) | 15.60 (7.05) | 8.78 (1.87) | 8.41 (1.81) | 9.81 (2.01) | 6.86 (1.36) |
| Axial compression force | 8.34 (5.25) | 6.35 (3.81) | 5.30 (3.18) | 4.72 (2.67) | 5.56 (2.64) | 6.80 (3.78) | 23.15 (14.7) | 40.09 (19.7) |
| Mediolateral shear force | 11.74 (8.05) | 9.72 (5.60) | 7.92 (5.39) | 7.36 (4.16) | 6.51 (4.32) | 6.86 (5.58) | 15.21 (13.6) | 12.25 (8.7) |
| Anteroposterior shear force | 6.52 (4.39) | 5.27 (3.31) | 4.69 (2.81) | 4.38 (2.43) | 5.03 (2.26) | 6.76 (3.94) | 25.02 (17.0) | 36.36 (18.2) |

**Table 3:** Inertial motion capture with predicted ground reaction forces (IMC-PGRF) and optical motion capture with predicted ground reaction forces (OMC-PGRF) versus optical motion capture with measured ground reaction forces (OMC-MGRF) for symmetrical lifting (SYM) with 5, 10, 15 and 20 kg, asymmetrical lifting (ASYM) with 5 and 10 kg as well as one- (TRA-OH) and two-handed transferring (TRA-BOX). ICC = Intraclass correlation coefficient (mean), RMSE = root mean square error (%BW) (mean ± SD), and rRMSE = relative root mean square error (%) (mean ± SD). Results are for the erector spinae muscle force.

| | SYM-5 | SYM-10 | SYM-15 | SYM-20 | ASYM-5 | ASYM-10 | TRA-BOX | TRA-OH |
|---|---|---|---|---|---|---|---|---|
| **Erector spinae force** | | | | ICC | | | | |
| IMC-PGRF vs. OMC-MGRF | 0.78 | 0.84 | 0.83 | 0.74 | 0.94 | 0.90 | 0.78 | 0.64 |
| OMC-PGRF vs. OMC-MGRF | 0.95 | 0.97 | 0.98 | 0.98 | 0.98 | 0.98 | 0.90 | 0.62 |
| | | | | RMSE | | | | |
| IMC-PGRF vs. OMC-MGRF | 20.35 (11.91) | 26.70 (12.34) | 28.23 (14.27) | 32.52 (18.83) | 13.46 (6.33) | 20.84 (8.78) | 14.69 (8.83) | 14.32 (10.38) |
| OMC-PGRF vs. OMC-MGRF | 8.53 (4.19) | 7.87 (3.75) | 7.75 (4.30) | 7.29 (3.58) | 6.16 (2.93) | 8.16 (4.64) | 8.69 (8.66) | 13.76 (6.72) |
| | | | | rRMSE | | | | |
| IMC-PGRF vs. OMC-MGRF | 24.84 (26.61) | 23.34 (13.41) | 21.75 (11.50) | 23.94 (14.05) | 11.33 (5.70) | 17.60 (9.52) | 47.60 (35.77) | 47.33 (34.36) |
| OMC-PGRF vs. OMC-MGRF | 7.82 (4.84) | 5.93 (3.36) | 5.26 (3.23) | 4.72 (2.57) | 5.26 (2.55) | 6.29 (3.45) | 21.29 (17.53) | 42.90 (18.32) |

**Table 4:** Median, 5$^{th}$ percentile and 95$^{th}$ percentile comparing inertial motion capture with predicted ground reaction forces (IMC-PGRF) versus optical motion capture with measured ground reaction forces (OMC-MGRF) and optical motion capture with predicted ground reaction forces (OMC-PGRF) versus OMC-MGRF for symmetrical lifting (SYM) with 5, 10, 15 and 20 kg, asymmetrical lifting (ASYM) with 5 and 10 kg as well as one- (TRA-OH) and two-handed transferring (TRA-BOX). Results are for L4-L5 axial compression force (%BW).

| | SYM | ASYM | TRA-BOX | TRA-OH | Overall |
|---|---|---|---|---|---|
| **OMC-MGRF versus IMC-PGRF** | | | | | |
| Median | 12.00 | -16.43 | -13.00 | -47.50 | -10.00 |
| 5$^{th}$ percentile | -118.83 | -105.16 | -91.31 | -145.84 | -111.28 |
| 95$^{th}$ percentile | 160.90 | 91.80 | 82.30 | 37.85 | 123.01 |
| **OMC-MGRF versus OMC-PGRF** | | | | | |
| Median | 12.00 | 5.65 | 4.18 | -10.73 | 6.45 |
| 5$^{th}$ percentile | -7.59 | -12.14 | -69.00 | -72.27 | -23.10 |
| 95$^{th}$ percentile | 37.60 | 29.14 | 31.57 | 6.03 | 34.02 |